**SANDIA REPORT**
SAND2010-6426
Unlimited Release
Printed September 2010

# Novel Detection Methods for Radiation-Induced Electron-Hole Pairs

Michael J. Cich, G. Allen Vawter, M. John Martinez, Christopher D. Nordquist, Mark S. Derzon

Prepared by
Sandia National Laboratories
Albuquerque, New Mexico 87185 and Livermore, California 94550

Sandia National Laboratories is a multi-program laboratory managed and operated by Sandia Corporation, a wholly owned subsidiary of Lockheed Martin Corporation, for the U.S. Department of Energy's National Nuclear Security Administration under contract DE-AC04-94AL85000.



Issued by Sandia National Laboratories, operated for the United States Department of Energy by Sandia Corporation.



Available to DOE and DOE contractors from
U.S. Department of Energy
Office of Scientific and Technical Information
P.O. Box 62
Oak Ridge, TN 37831

Telephone: (865) 576-8401
Facsimile: (865) 576-5728
E-Mail: reports@adonis.osti.gov
Online ordering: http://www.osti.gov/bridge

Available to the public from
U.S. Department of Commerce
National Technical Information Service
5285 Port Royal Rd.
Springfield, VA 22161

Telephone: (800) 553-6847
Facsimile: (703) 605-6900
E-Mail: orders@ntis.fedworld.gov
Online order: http://www.ntis.gov/help/ordermethods.asp?loc=7-4-0#online

SAND2010-6426
Unlimited Release
Printed September 2010

# Novel Detection Methods for Radiation-Induced Electron-Hole Pairs

Michael J. Cich[a], G. Allen Vawter[a], M. John Martinez[a], Christopher D. Nordquist[a], Mark S. Derzon[b]
[a]RF/Optoelectronics (1742) and [b]Advanced MEMS (1749-2) Departments
Sandia National Laboratories
P.O. Box 5800
Albuquerque, New Mexico 87185-MS1085

**Abstract**

Most common ionizing radiation detectors typically rely on one of two general methods: collection of charge generated by the radiation, or collection of light produced by recombination of excited species. Substantial efforts have been made to improve the performance of materials used in these types of detectors, e.g. to raise the operating temperature, to improve the energy resolution, timing or tracking ability. However, regardless of the material used, all these detectors are limited in performance by statistical variation in the collection efficiency, for charge or photons. We examine three alternative schemes for detecting ionizing radiation that do not rely on traditional direct collection of the carriers or photons produced by the radiation. The first method detects refractive index changes in a resonator structure. The second looks at alternative means to sense the chemical changes caused by radiation on a scintillator-type material. The final method examines the possibilities of sensing the perturbation caused by radiation on the transmission of a RF transmission line structure. Aspects of the feasibility of each approach are examined and recommendations made for further work.

## ACKNOWLEDGMENTS

I would like to thank Olga Spahn (1742) for encouragement in starting this work. I would also like to thank Lorraine Sadler (8132) for hosting my visit to the Sandia-California site to learn about their work on radiation detection using the electro-optic effect.

# CONTENTS



# FIGURES

# 1. INTRODUCTION

Radiation detectors have long looked to improve performance by engineering material properties and detector geometry to improve the collection of carriers generated during the stopping of high energy particles in the detector volume. The spectroscopic information about the incoming radiation energy is contained in the number of carriers collected per particle of radiation, so detector materials require both high stopping power for the incident radiation and excellent carrier transport. This report investigates new sensing mechanisms that can detect radiation-induced carriers immediately after generation, without requiring the transport and collection of these carriers. Note that scintillators also face transport and collection issues.

A number of candidate solid state radiation detector materials offer clear improvements over commonly used germanium and silicon detectors. These advantages may include higher resolution, higher sensitivity, smaller detector volumes, or uncooled operation. For gamma detection, the theoretical improvement of these candidate materials is due to higher average Z and larger bandgap, for example in CdTe materials. Unfortunately, bringing the electrical performance of these candidate materials to the level of single crystal germanium, which has had decades of extensive development, is a barrier that may be insurmountable.

There are means other than charge or luminescence to detect the carrier generation pulse associated with the radiation-matter interaction. For instance, the generated carriers can result in a transient change in the complex refractive index. The material development then only has to optimize optical performance, which may be more forgiving of material defects than electrical performance. Alternatively, the use of RF/microwave signals to measure the transient changes in local dielectric properties offers another frequency band in which the radiation induced signal can be detected without the background associated with the essentially dc-coupled standard charge signal. *This study examines possible methods to leapfrog the common electrical transport roadblock in new material development by identifying new options for signal readout.*

When high energy radiation enters a material, it loses its energy through electronic and nuclear stopping, resulting in highly energetic ions and excited electrons in a "track" with micron-scale diameter and tens to hundreds of microns length, depending on the material and the energy of the radiation. The duration of this disturbance is on the $10^{-10}$ s timescale. In standard detectors, this charge diffuses, drifts, and recombines on its path to being collected by electrical contacts on a nanosecond or longer timescale; see Appendix D of the text "Radiation Detection and Measurement' by G. Knoll, Ed. 3 on p.790 for details of this process. This process by itself generates resolution broadening. Indeed, coupling multiple wire proportional counters with optical interrogation enhances resolution as does dividing a sensor into pixels (Knoll). The hypothesis is that we can determine the number of electron-hole pairs directly and avoid traditional resolution and temporal broadening caused by Shockley-Ramo methods for radiation tracking and signal readout; this would enable new performance measures and improved metrics for radiation sensing.

The first alternative interrogation method (Section 2) is based on the years of development of high speed optoelectronics. We will explore the suitability of compound semiconductor photonic integrated circuits as radiation-induced transient charge detectors. One of the most

sensitive optical sensor configurations is the balanced Mach-Zehnder interferometer with ring resonators in each arm to improve the phase modulation figure-of-merit. Within these structures we expect that alpha, beta, or lower energy gamma radiation will create roughly $10^5$-$10^6$ electron-hole pairs (EHP) within a few-micrometer cubic volume. The resulting complex refractive index changes due to local EHP generation will be modeled in a time-domain travelling-wave scheme to understand the response of various ring resonators to localized EHP generation. The simulation will allow us to explore different sensor designs and place bounds on the performance of these photonic circuits as radiation sensors.

A major concern for sensing neutrons with this method is the low interaction of neutrons with compound semiconductor materials, and the low sensing volume associated with planar waveguides. One possible solution is to include a neutron capture material as an overlayer, such as a heavily boron-doped glass or even boron nitride. Alternatively, the waveguide can be made with lithium niobate or related materials. $^6$Li has a large cross section for neutron capture. Detailed sensor design to optimize/compare performance in different materials will require further work. In this study we limited ourselves to basic studies to determine if the proposed sensing concept merits further investigation.

There is an ongoing NA22 project at Sandia–California to develop an electro-optical detector for radiation (PI: Lorraine Sadler, 8132). That project is using imaging techniques to identify, in real time, optical scattering from neutron-generated tracks in KDP and other materials with a high electro-optic coefficient. Like this proposal, they are motivated by the fact that materials with a high neutron cross-section are not great at electrical transport but may have other properties, such as the electro-optic coefficient, that can be exploited for neutron sensing. However, we are taking a broader look, using the other method, described above, to sense localized charge generation, with the goal of taking advantage of Sandia's expertise in photonic integrated circuits and RF/microwave technology.

A second option for direct sensing of radiation trails without traditional readout is to use RF/microwave measurements (Sections 3 and 4). This concept simply takes advantage of the fact that a line of charges in a time-oscillating field can alter the response of a circuit. As with the optical interrogation method above, the technology behind the measurement is highly sophisticated thanks to its application in communications. The detection medium is even more flexible, thanks to the wide range of frequencies (0.1-100GHz) that could be employed. In fact, it may be possible to demonstrate the readout technology using a known strongly-interacting medium (such as 3He, or KDP as mentioned above) as a dielectric. We simulate the best geometry to couple a radiation-induced charge trail into a RF/microwave circuit, identify noise sources, and look at what kind of amplification and filtering can be used to improve the signal-to-noise. With Sandia's investment in wafer-scale packaging, there may be a realistic path to create a large 2-D array of amplifiers and circuitry should the simulations prove the advantages of RF/microwave charge detection over traditional readout.

# 2. RESONANT PHOTONIC INTEGRATED CIRCUIT FOR RADIATION DETECTION

The prime issue explored by this study is the practical implications of using local generation of free carriers by an ionizing radiation event to alter the properties of an optical circuit in an observable manner. Furthermore, it is desired to forgo the need to actually collect generated local charge for electrical measurement by taking advantage of the nearly instantaneous change of the complex optical refractive index in response to changes in the free-carrier concentration and to use local changes in the refractive index as a means to modulate light in a photonic circuit.

The alteration of local refractive index in direct-gap compound semiconductors is, for practical purposes, instantaneous and depends mainly on the electron and hole effective masses, the light wavelength, the non-modulated refractive index at the light wavelength, as well as the concentration of free electrons and holes [1]. The relationship is written as

$$\Delta n = \frac{q^2\lambda^2}{8\pi^2 n\varepsilon_o c^2}\left(\frac{N}{m} + P\frac{m_{lh}^{1/2} + m_{hh}^{1/2}}{m_{lh}^{3/2} + m_{hh}^{3/2}}\right)$$

In this relation, N and P are the local density of electrons and holes, respectively. m is the electron reduced mass, $m_{lh}$ and $m_{hh}$ are the light and heavy hole reduced masses, q is the electronic charge, $\lambda$ the wavelength, n the base refractive index, $\varepsilon_o$ the vacuum permittivity, and c the speed of light.

In order to explore the sensitivity of a photonic waveguide-type sensor exploiting free carrier modulation of local refractive index, a highly sensitive, balanced, optical interferometer is desired. For this purpose we have selected an integrated ring-assisted Mach-Zehnder interferometer (MZI) with a ring-type resonator coupled to one arm [2, 3]. The configuration is illustrated in Fig. (1) where we see a depiction of a conventional waveguide-type MZI with a ring resonator coupled to the upper arm. A small region highlighted in magenta illustrates the region to be exposed to ionizing radiation capable of creating electron-hole pairs in the semiconductor. Details of ring-assisted MZI operation can be found in the references. Here we highlight the particular features making these structures attractive as radiation sensors.

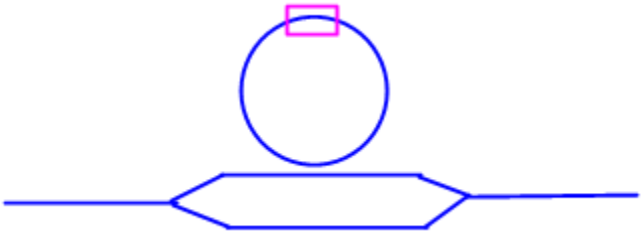

**Figure 1.** Illustration of a ring-assisted MZI sensor. Blue lines are optical waveguides in a PIC. Light is incident from either the left or right sides and exits from the opposite side. The magenta box defines the free-carrier modulation region described in the text.

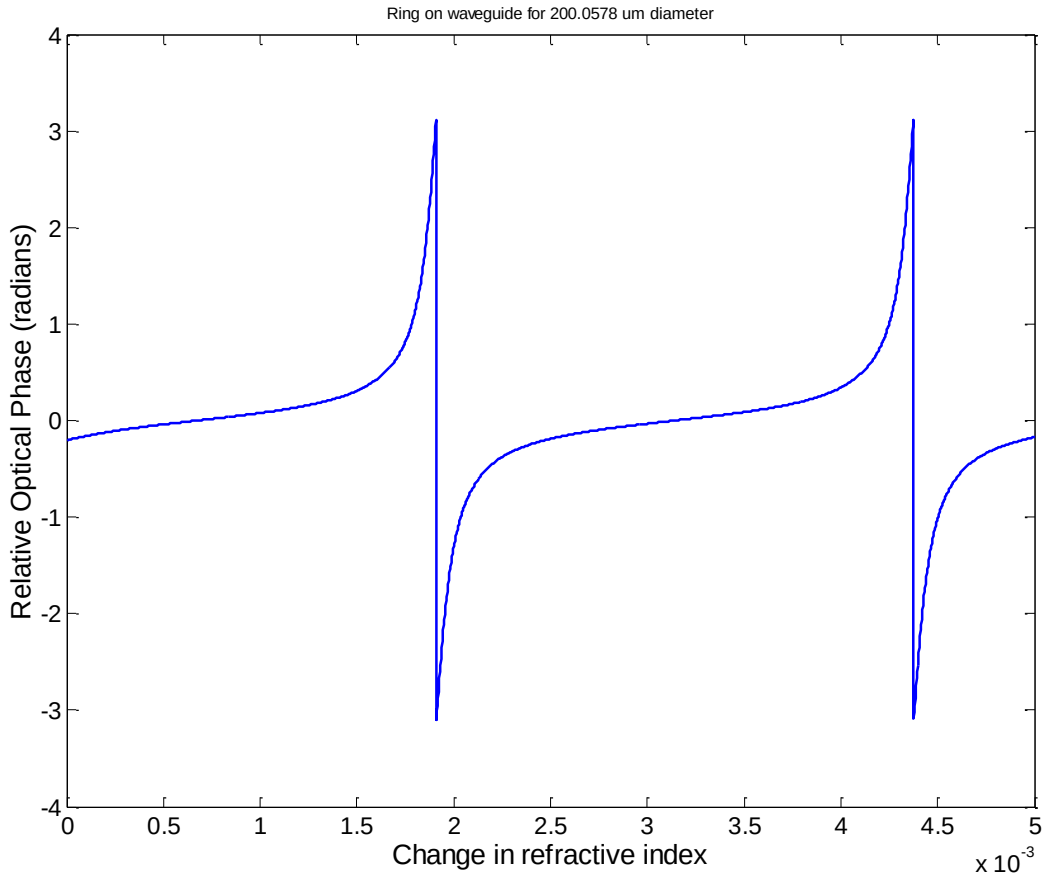


**Figure 2.** Relative optical phase of light in a straight waveguide passing a coupled ring resonator. The simulation is structured so that as the refractive index of the ring is adjusted it passes through two optical resonances, where the optical path length of the ring is an integer multiple of 2πλ. At the resonant condition the optical phase of light passing the ring quickly shifts by 2pi.

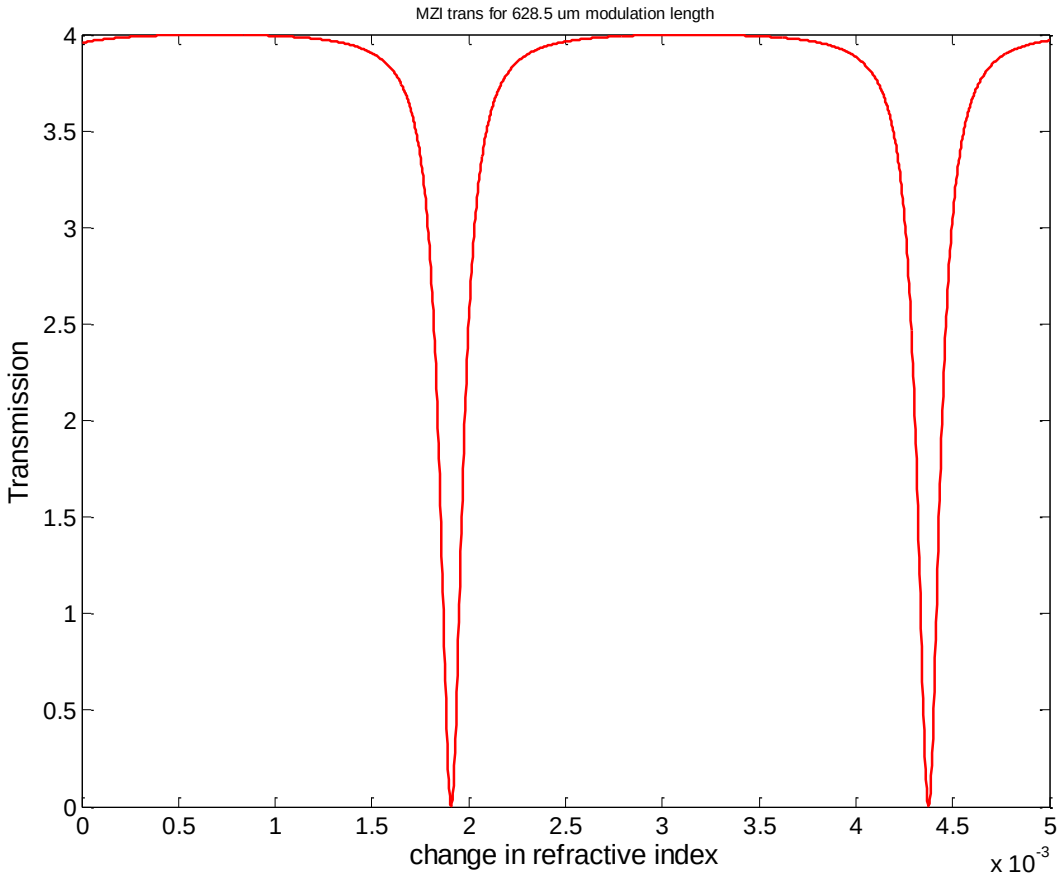


**Figure 3.** Modulation of optical intensity through a ring-coupled MZI for the same conditions used in the calculation of optical phase in Fig. (2).

The basic principle of a ring resonator coupled to an optical waveguide is shown in Figure 2, showing the relative optical phase of light passing through a waveguide optically coupled to a ring resonator. The simulation is structured so that as the refractive index of the ring is adjusted it passes through two optical resonances, where the optical path length of the ring is an integer multiple of $2\pi\lambda$. At the resonant condition the optical phase of light passing the ring quickly shifts by $2\pi$. This rapid phase change can be measured by placing the ring-coupled waveguide in an MZI where light in the reference arm of the MZI is coherently combined with light from the ring-coupled arm causing the MZI to flip from "on" to "off" and back "on" again as the phase of the ring-coupled arm cycles through a $2\pi$ phase shift. The rapid transition of the MZI through a resonant "off" state is shown in Fig. (3) for the same conditions used in the calculation of optical phase in Fig. (2). The important characteristic to note here is that a properly designed ring-assisted MZI is capable of rapid on-off transitions with very small refractive index changes. As a result, these structures are highly interesting as optical sensors [3]. It is the focus of the remainder of this section of the report to show results of a quantitative simulation of ring- and disk-assisted MZIs designed for best sensitivity to small changes in the density of free carriers in a small material volume consistent with a single-particle interaction.

The ring-assisted MZI sensor used in these simulations comprises an InGaAsP-type PIC with single-mode optical waveguides designed nominally for 1.55 um wavelength light. The optical splitter and combiner at each end of the MZI is assumed to be an ideal, lossless, equal power split. All waveguides use a loss of 0.9 dB/cm with no consideration of power coupled to radiation modes at bends. In order to simulate single-particle or single-photon events a small region is defined as having a modulated free-carrier concentration, this is depicted as the magenta region in Fig. (1). Since the simulation is one-dimensional only a length of interaction region is defined. The implicit assumption is that carrier concentrations are uniform across the 1-5 um width of the optical mode. In all cases we assume 5% guide-to-guide power coupling at the evanescent optical directional coupler used to couple light circulating within the ring to the straight waveguide.

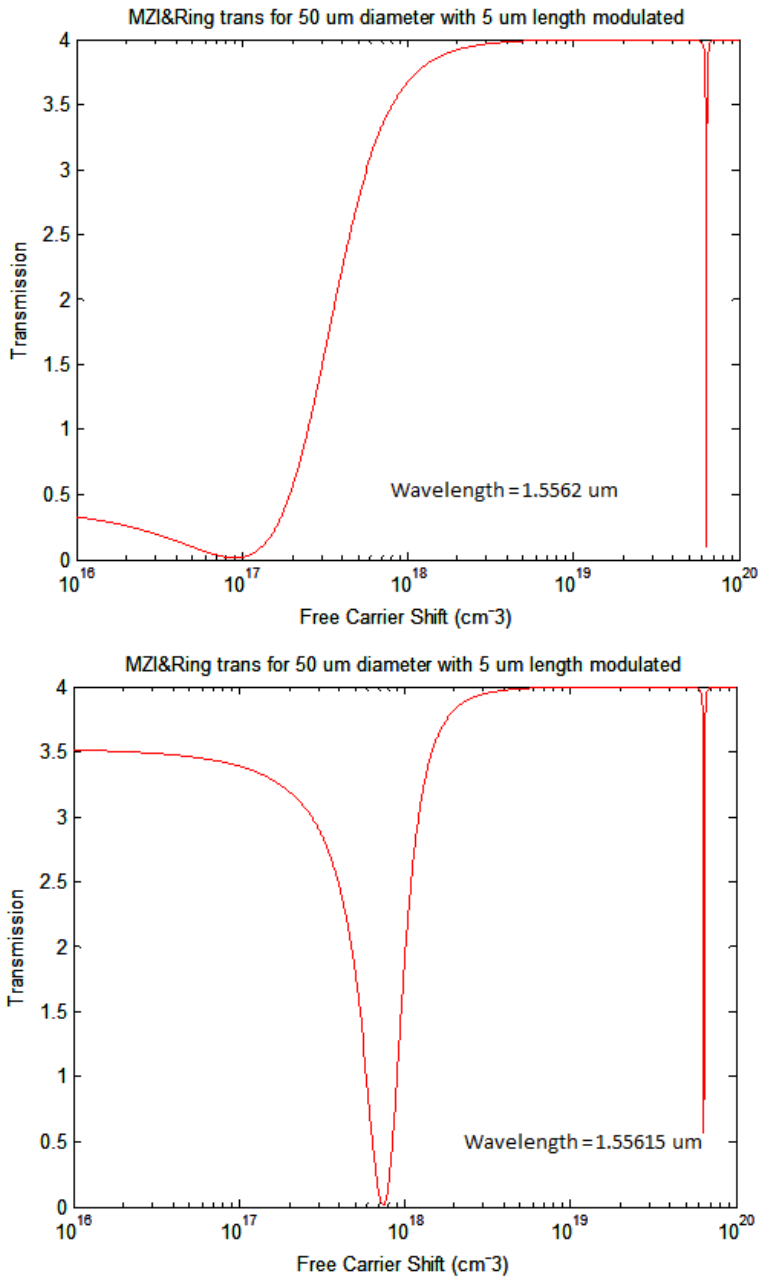


**Figure 4.** Light transmission through a ring-assisted MZI as a function of free-carrier concentration in a 5 um long section within a 50 um diameter ring. Insets show the wavelength of light. The upper and lower figures differ only in the wavelength of light used.

Simulation results for a 50-um diameter ring with a 5 um long modulated section are shown in Fig. (4). Operation of the sensor at two different wavelengths (inset) is shown in the upper and lower portion of the figure. In the top figure an abrupt "off" to "on" switching of light transmission through the entire sensor is seen at free-carrier concentrations in the mid-1e17 $cm^{-3}$ range for 1.55620 um wavelength. If the wavelength is adjusted to 1.55615 um the sensor switches to a more resonant behavior with an off-state dip near 8e17 $cm^{-3}$.

Clearly the ring-assisted MZI can be made sensitive to fairly moderate changes in free-carrier concentration. Equally interesting is that the sensor operation can be wavelength tuned from a thresholded on-off type, as in the top of Fig. (4), to a precise resonant output at a specific free-carrier concentration (bottom of Fig. 4). Adding electro-optic modulators to the rings will allow for electrical tuning of the ring effective optical diameter. Doing so will permit adjustment of sensor operation for wavelength drift and thermal variation.

In order to explore smaller structures suited for fabrication as 2-dimensional arrays of closely spaced sensitive "pixels" a disk-assisted MZI was simulated. In the design the ring was replaced with a 10 um diameter disk. The disk configuration is needed to reduce optical losses in such a small ring cavity but does not alter the concept of the sensor beyond allowing for a smaller physical structure.

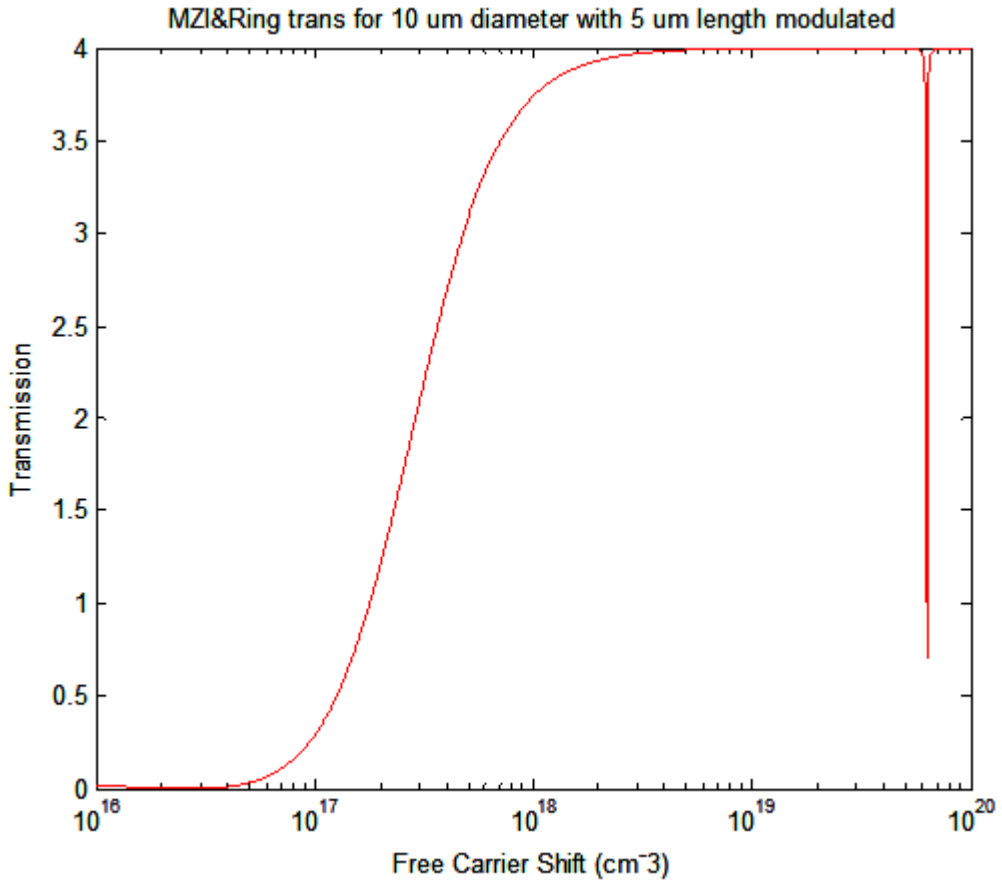


**Figure 5.** Light transmission through a disk-assisted MZI as a function of free-carrier concentration in a 5 um long section within a 10 um diameter disk. Wavelength of light is 1.54662 um.

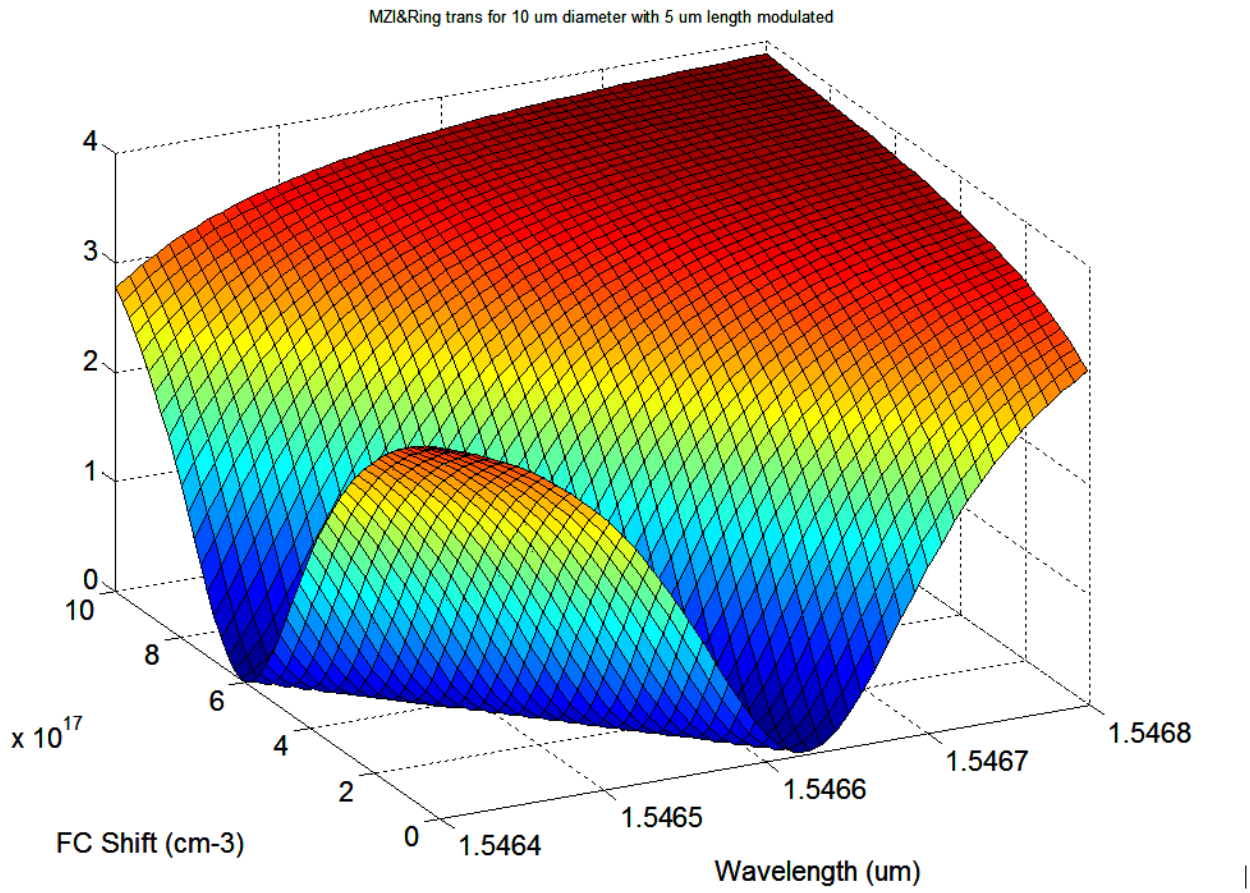


**Figure 6.** Light transmission through a disk-assisted MZI as a function of free-carrier concentration and wavelength of light within a 10 um diameter disk. Free carrier concentration is altered only with a 5 um long section of the disk.

Simulation of a disk-assisted MZI is shown in Fig. (5) where a disk diameter of 10 um is used along with the same 5 um interaction length. Similar performance is seen as in the case of the 50 um ring with the off-on switching occurring for slightly lower free carrier concentrations.

As suggested in the discussion above, these resonant MZIs are sensitive to variations in wavelength. This is illustrated in Fig. (6), where transmission through the disk-assisted MZI of Fig. (5) is shown as a function of both free-carrier shift and wavelength. As seen in the figure, sub-nm control of wavelength is required to use these devices without additional feedback stabilization. We can, however, imagine that wavelength tunable lasers are used with these sensors such that the laser wavelength is tuned to a notch in the sensor response (e.g., the notch in the bottom of Fig. (4)) and a feedback loop constructed forcing the laser wavelength to track the sensor notch. In this manner the presence of ionizing radiation manifests itself as a sudden detuning of the sensor and a corresponding change in the feedback signal. (This is very similar to techniques used in modern optical navigation gyros.)

In order to completely model ring-assisted MZIs as ionizing radiation sensors the density and distribution of free-carriers generated by interactions with energetic particles and photons needs to be computed. While we have taken care to assure that the sensor volumes used are consistent

with single-particle interactions, a detailed examination of carrier density and distribution has fallen beyond the scope of this late-start LDRD.

In summary, ring- and disk-assisted MZIs have been explored as potential ionizing radiation sensors where localized changes in free-carrier concentration caused by ionizing particles are sensed using local instantaneous changes in the refractive index. Such a structure does not require transport of generated carriers to collection contacts or capacitor plates and so is essentially immune to carrier lifetime and transport effects. It has been shown through optical simulations of representative 1D structures that ring and disk assisted MZI can be made sensitive to free-carrier concentrations as low as ~1e17 $cm^{-3}$. A wavelength feedback configuration has been proposed to stabilize the sensor against wavelength drift due to temperature or electrical bias variations.

With respect to use as a radiation detector, we note that 1MeV gamma radiation result in a linear energy transfer and free charge creation rate of approximately $10^5$/cm or 10 electron-hole pairs per micron – a carrier density of approximately $10^{14}/cm^3$ , about 3 orders of magnitude too low for detection in the proposed device. On the other hand, a 1 MeV alpha will deposit its energy over about 5 microns leading to a carrier concentration of ~2e18/$cm^3$. An experiment could be devised to detect alpha particles using this device.

# 3. ELECTRON SPIN RESONANCE TECHIQUES FOR RADIATION DETECTION

Electron spin resonance (ESR, equivalently electron paramagnetic resonance, EPR) techniques have been used extensively in chemistry, biology, medicine, and physics since their development in the 1940s. In a typical system the sample sits in a microwave resonant cavity in a magnetic field. The magnetic field is used to split the degenerate energy levels of a paramagnetic center. At a particular magnetic field, the energy level splitting matches the energy of the incident microwaves and there is increased microwave absorption. This absorption can be used to identify the chemical structure and concentration of the responsible center.

Note that the difference between EPR and nuclear magnetic resonance is the use of unpaired electron spins vs. unpaired nuclear spins. Almost every element has at least one isotope with unpaired nuclear spins, but unpaired electrons occur in relatively few molecules due to the lowering of bond energy achieved by pairing electrons. Also, the much larger moment of an orbital electron compared to nuclear magnetic moment results in roughly 1000x increased energy level splitting for a given magnetic field. Therefore, EPR can use a much smaller applied magnetic field for a given microwave frequency, and usually presents a much less complicated spectrum for analysis.

The use of the EPR method for radiation measurements is already well established. It is routinely used for x-ray radiation dosimetry using alanine dosimeters. It has also been developed as a means to assess accidental exposures through measurements on tooth enamel. Both of these applications make use of the fact that stable paramagnetic species are generated as a result of exposure of these materials to x-rays. By measuring the total concentration of the paramagnetic species, the total exposure can be determined. The resolution of these dosimeters has been demonstrated down to 5 mGy [4]. Unfortunately, for detecting single events, say 100 keV deposited in a 1 gram detector, the sensitivity would have to be $1.6 * 10^{-8}$ mGy – an improvement of over 8 orders of magnitude. Given that a substantial averaging time (many seconds) was used to achieve 5 mGy resolution in alanine, it is clear that the EPR technique lacks the sensitivity to replace charge collection based radiation detection methods; EPR sensitivity is on the order of $10^{11}$ spins/sample, whereas the resolution needed to displace germanium detectors is on the order of 100 spins.

In optically detected magnetic resonance (ODMR), an optical signal is used to monitor the magnetic resonance condition. Spin selection rules dictate that the recombination can only occur between states with no net change in spin. Therefore, changes in the polarization or intensity of emitted light indicate a change in the population of spin singlet (S=0) vs. triplet (S=1) states. (After recombination, S=0, so recombination from the triplet state is forbidden by the selection rules). Under magnetic resonance conditions, the microwave field introduces spin flips, so that the population of triplet states increases and the emitted light decreases.

The great advantage of ODMR over EPR is an enormous increase in sensitivity. This improvement is fundamentally due to very effective isolation of the microwave photons causing the excitation from the optical photons comprising the probe beam. ODMR techniques have undergone significant development recently for single spin readout for quantum computing

applications. These experiments take advantage of two tricks to obtain sensitivity to a single defect: very low temperatures to limit thermally-induced spin flips and allow longer measurement times, and restriction of the background by limiting the active volume using confocal microscopy, masking, or scanning probe techniques. Unfortunately, both of these methods are undesirable in a radiation detection application; low temperatures add to size, weight and power requirements, and the active volume that has to be interrogated is set by the interaction length of the radiation of interest in the sensing material, typically on the order of a >0.1 mm. However, Anisiriov et al. was able to show ODMR at room temperature with a sample volume of 1 mL to detect short-lived hexafluorobenzene radicals generated by beta-radiation of a dilute solution in squalane [5]. Based on their source activity, the yield of radicals from the radiation, and the lifetime of the radicals before recombination, they estimated their signal was due to a steady-state concentration of about 20 excited molecules in the sample volume. This demonstrates the sensitivity needed for use as a radiation detector. Since then, ODMR has been used extensively with biological samples to trace reaction kinetics, particularly in studies of photosynthesis.

Unfortunately, while the ODMR method can be used to track the kinetics of multiple chemical species (through their different g-values) following an excitation, there is no performance advantage over scintillators, because the ODMR signal arises from the light emitted during the final recombination of the excited species – one photon (at best) per excitation. What is needed is a method to sensitively detect the presence of radical species produced by radiation. Ideally, these species would be short-lived, so that the material returns to a low-background state following each detection event. Then we will need to detect the concentration of radicals in a time-resolved fashion and without the benefit of lock-in techniques due to the unknown and random arrival times of radiation.

In order to remove the single-excitation – single-photon constraint that would limit ODMR performance to the current performance of scintillators, a detection method for the excited species that doesn't rely on the destruction of the excited state for readout is needed. A strong candidate is Raman scattering, particularly coherent Raman scattering for enhanced background rejection. This has been developed recently for gas phase concentration measurements, but can be applied to solids and liquids as well [6]. A particular advantage lies in the fact that the coherently scattered Raman photon is emitted in the same direction as the probe beam, unlike scintillator luminescence which may be emitted at any angle, thereby increasing the collection efficiency of the signal. Coherent anti-Stokes Raman scattering (CARS) has been extensively studied for biological imaging. The coherent scattering is typically set up using two input lasers with frequencies separated by the frequency of a Raman mode. Alternatively, the conditions needed for coherent scattering could be set up by an applied magnetic field to separate degenerate triplet energy levels by the amount of an applied microwave photon energy, e.g., roughly 3350 G for 9.4 GHz microwaves. Note that the nuclear resonance could be used as well in proton-rich materials for neutron detection – requiring 14.3 MHz excitation at the 3350G applied static field. Organic scintillator materials are particularly good candidates for testing this technique, because they have reasonably long-lived excited intermediates. Furthermore, the standard scintillation signal would allow a means of coincidence detection of the Raman signal. There is also the possibility that the Raman spectrum would give information on the creation of

multiple excited species, whose relative abundance was a function of the incident radiation, allowing neutron/gamma discrimination.

A major impediment to Raman techniques is the need for high laser powers to overcome the very small Raman cross-section. The availability of fiber lasers has brought Raman into many commercial applications, and Raman spectroscopy systems for routine quality control are now available.

The application of CARS to transient excited state spectroscopy has already been demonstrated using Rhodamine 560 dye with ~10 ps time resolution [7]. In that case the measurement could be synchronized to the excitation. The radiation detection case doesn't allow control over the excitation timing, but we are free to pick a sensing material with the largest possible Raman signal from the excited states, while matching the need for a reasonable radiation cross-section.

To summarize this section, we find that standard microwave resonance techniques, in which the direct absorption of microwaves is measured, are insufficiently sensitive –by many orders of magnitude - to be used in direct radiation detection. There is no obvious route to increase the sensitivity sufficiently from the level of alanine dosimeters. Specialized magnetic resonant techniques, such as optical detection of magnetic resonance, can have the needed sensitivity. However, they ultimately depend on the emission of a photon from an excited state, and the resonance is indicated by a change in the probability of this emission under a combined magnetic and microwave field. Therefore, they can only have the performance at best equal to a scintillator, assuming each detection material can be equally optimized, while having substantially more complexity.

The only alternative technique we found which offers the sensitivity needed for single-event radiation detection is CARS. The sensitivity was reported as $10^5$ vibrational states in 2006 [8]. This will need to be improved by at least an order of magnitude to be competitive with current resolutions available with charge-collection radiation detection methods. There have been no reports on using CARS for radiation detection to date, but transient measurements on excited states have been performed. Furthermore, there are possibilities to extract more information about the incoming radiation direction using the dependence of excited state yield on the incoming radiation direction, or by directly probing where in the material excited states exist. CARS is particularly amenable to rapid 3-D imaging through beam scanning, since the two-beam CARS method only delivers a signal from the volume where both beams overlap.

# 4. RF STRIPLINE TECHNIQUES FOR RADIATION DETECTION

*Hypothesis Development of the Need for High Bandwidth Sensing*

The output pulse from ionization chambers, proportional counters and Geiger counters is generally considered to form when charge is collected on the electrodes. That model implies a delay based on charge motion. See discussion in Appendix D of Knoll. In that model the charges are collected thru the induced charge mechanism and are generally well modeled by the Shockley-Ramo theorem.

The Shockley-Ramo theorem holds that the instantaneous current at the induced at the electrode is equal to:

$$i = q\vec{v} \times \vec{E}_0$$

Where $q$ is the charge of the carrier, $v$ is the velocity and $E_0$ is the the weighting field. In this case the current obtained is due to the charge separation and acquisition at the electrode. This is a long process generally with timescale (ns to microsceconds are typical) driven by the mobility and the characteristics of the charges moving along the field lines. By its very nature the charge drifting and induced charge model is not a prompt phenomenon and is not complete.

Induced charge collection is not the entire story. It is well known that the pulse begins at the time the charged particle deposits its energy rather than at the time the charge has drifted to the electrodes. The charges deposit their energy in nominally 200 ps while the ionizing particle is slowing down. The charges do not have time to separate or to drift far in that time frame. The hypothesis we have is that those charges, prior to separation by the field, affect the charge distribution on the electrodes and hence capacitance in the system.

Our hypothesis is that this early time distribution creates a reordering of charge at the electrode through the displacement current. This nearly instantaneously affects the charges at the electrodes for the displacement current must rearrange the charges at the electrodes to mirror the the effect of the charge particle trail. This affects the capacitance of the system and the voltage across the plates. In Figure 7 we show a simple small pixel where an ionizing particle is creating the early time charge carrier distribution. What we will do next is develop a framework for modeling the amplitude of the effect and design an experiment to motivate an attempt to measure it.

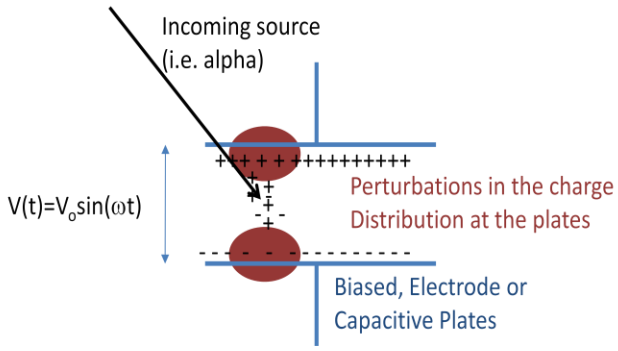


**Figure 7.** Schematic of early portion of ion trail, prior to separation of charge and collection at the electrodes.

A complete derivation would start at Maxwells equations, walk through Gauss's law and then arrive at the displacement current equation:

$\nabla \cdot E = \frac{\rho_{free}}{\varepsilon}$ where ε is the permittivity of free space and it is 8.9e-12$C^2$/J-m or 55 electrons/V-micron. We wish to sense the nearly instantaneous number of free charges for a given ionizing particle rather than the free charge density $\rho_{free}$ but they are related. We now discuss how one would attempt to determine both.

In a planar capacitor the capacitance is determined by C=Q/V where Q is the charge on the plates and V is the applied voltage and the electric field is E=V/d where d is the distance between plates. The capacitance is given by $C=k\varepsilon A/d$. Here k is the relative permittivity, A is the area of the pixel and d is the separation between plates. Generally there is no free charge in the dielectric between the plates and the divergence of the electric field is zero. If the radiation creates a swarm of free charges then Maxwells equations, through the displacement current equation gives a δC or δQ perturbation to be measured. As the radiation slows down and creates the charge trail the associated parameters are:

$$\frac{dC(t)}{dt} = f_s * \frac{dQ(t)}{dt} / V(t)$$

and

$$dQ(t) = LET(E) * v * dt$$

where dC(t)/dt is the instantaneous change is capacitance, $f_s$ is a screening factor, dQ/dt is the rate of electron-hole creation and V(t) is the applied voltage, the LET(E) is the linear energy transfer (LET) in hole-pairs/micron at the ionizing radiation current energy.

The number of charges or electron-hole pairs is determined by the interaction of the ionizing particle with the sensor medium. Table 1 gives some of the key parameters for stopping in a silicon and liquid Xe media [9-12] using $\rho_{si}$=2.3g/cc and $\rho_{Xe}$=3g/cc. These numbers are averaged over the particles stopping.

**Table 1.** Range and Deposition Rates for Liquid Xe and Si.

| | Range (micron); 5 MeV alpha | electron-hole pairs (5 MeV alpha | Electron-hole pairs/μm for a 1 MeV electron | Energy per electron hole pair |
|---|---|---|---|---|
| Silicon | 23 | 6e4 | 9 | 3.7 |
| Xe | 37 | 9e3 | 3e1 | 15 |

dQ varies from 9 e-h pairs/micron to roughly 6e4e-h pairs/micron. Note that the difference between particle types is much larger than the difference between materials.

In the 1D geometry of Figure 7 the relationship between the applied voltage and the capacitance is determined by *Q=V*k*epsA/d.* The parameter to measure then becomes the perturbed capacitance or the perturbed amount of charge and this measurement needs to be made in the nominal 200 ps of the slowing of the ionizing radiation. This makes it a nominally 5-15 GHz measurement.

The value of dQ is basically fixed by the radiation and the relative capacitance of an unperturbed pixel is determined by the geometry. We explore the parameter space in Table 2. Table 2 compares dQ/Q for electrons and alphas stopping in two different size pixels. These are a 300x300x20 μm pixel and a 20x20x20 μm pixel. The capacitance, assuming k=1 for both, is approximately 0.04 pF and 2e-4 pF respectively. Obviously these are small and likely can only be measured where the parasitic capacitance is small and well characterized.

**Table 2.** Estimated dQ/Q for different pixel designs.

| | Q=5e6e-s<br><br>[Pixel A=9e4 $\mu m^2$, d=20 μm; 10 V] | $dQ_{max}$ e-hole pairs; d=20 micron pixel; A=9e4$\mu m^2$ | dQ/Q | Q=2200e-‘s<br><br>[Pixel A=4e2 $\mu m^2$, d=20 μm, 10V] | dQ/Q; d=20 micron, A=4e2 $\mu m^2$ | |
|---|---|---|---|---|---|---|
| | | | | | | |
| **silicon** | | | | | | |
| Alpha | 5e6 e-hole | 6e4 | 0.1% | 1e4 | 400% | Range is longer than pixel |
| Electron | 5e6 e-hole | 9 | 2e-4% | 1e4 | 0.1% | |
| | | | | | | |
| **xenon** | | | | | | |
| Alpha | 5e6 e-‘s | 9e3 | 0.2% | 1e4 | 90% | |
| Electron | | 30 | 6e-4% | 1e4 | 0.3% | |

Measurements of capacitance are made in a few different ways. The first is a ‘direct’ measurement. The "direct" method charges the capacitor from a defined current source for a known time, then one measures the voltage across the capacitor. This method requires a very low current, high-precision current source, and a high-impedance input to measure the voltage [13]. This method does not lend itself to high rate changes and small dC/C. The second method uses the capacitor to create an RC oscillator, and then measures the time constant, frequency, or period. This method is simple, but it usually doesn't achieve high accuracy. Yet a third method, involves measuring the capacitor's ac impedance [14]. A sine-wave source excites the capacitance, and the capacitor's current and voltage are measured. Using a four-wire ratiometric connection to the capacitor, a synchronous demodulator then provides one of the most accurate results available. However, the circuit is very complex and has the highest part count or ability to resolve small dC/C. Utilizing an analogue to the last method above is likely the way to make this measurement.

Why hasn’t this been measured? Because it is hard – those capacitances and the signals are small and fast and no one has had the ability 1) to make the pixels and 2) to add the needed electronics, and 3) a fast enough oscilloscope. Now that we have completed this analysis of the signal amplitude and fractional capacitance change we can attempt to make a measurement.

Recently we have been doing some sensor development that may allow us to measure this phenomenon directly and to compare performance of this method to traditional induced charge readout performance. The lithographic fabrication techniques pursued in LDRD 10-0702 and LDRD 10-1025 for a massively pixelatted sensor may offer the potential to fabricate a small area

thin sensor that we can attach as a close couple, meaning low parasitic capacitive preamplifier. Unfortunately we were not able to complete the analysis in this LDRD. However, we now present additional RF performance calculations done to show the feasibility of radiation detection using this approach.

## Transmission Line Approach

The objective of this section is to examine methods by which changes in radio frequency (RF) properties may be exploited to create a new type of radiation detector. More specifically, the aim is to take advantage of temporary changes in material properties to which RF circuits may be sensitive such that it is not necessary to physically transport charge generated by radiation to detect it. Besides the very fast response time of such an approach, there is also a potential for making a detector with a relatively large detection volume that is limited by the interaction distances of electromagnetic fields rather than by solid state carrier transport distances which are generally much shorter.

The first approach considered involved the use of simple microstrip transmission lines, as illustrated in Figure 8. Because radiation-induced events can take place on time scales of less than 1 ns, it is expected that microwave frequencies up to 20 GHz would be necessary to resolve the events. GaAs was chosen as the microstrip substrate material, because is it well understood and known to be good choice for microwave frequencies. Since we are aiming for a detection volume with dimensions on the order of hundreds of microns, a relatively thick substrate, *h*, was chosen, which in turn would result in a larger transmission line width, *w*.

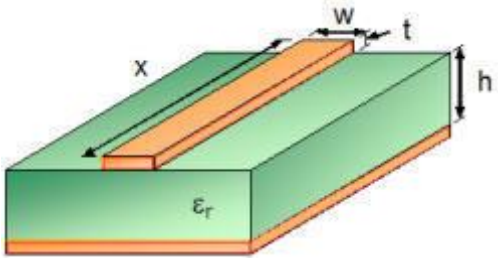


**Figure 8.** Illustration of microstrip transmission line [15].

For the sake of convenience a target impedance of 50 Ω was chosen, and transmission line width was calculated using the Agilent LineCalc™ application using the MLIN model with a relative dielectric constant (permittivity), $\varepsilon_r$, of 13.1 for GaAs [16], and a substrate thickness of 500 µm. The calculated line width for this impedance is 390 µm. This, then was used within the Agilent *Advance Design System* software package to simulate a piecewise transmission line modeled as two long sections joining to a short section with a different dielectric constant, as shown in Figure 9. In this model, the short section, labeled TL3, is a gross representation of the area affected by radiation interacting with the substrate, changing its effective dielectric properties through local ionization. The two long sections were chosen to be 500 µm (the simulations are insensitive to this value), while the short sections was arbitrarily chosen to be 10 µm in length. Clearly, such radiation would not affect the entire width of the transmission line, but this simulation was intended to see if there might be a detectable phenomenon with very optimistic assumptions before undertaking any more refined analysis.

The simulations focused on s-parameters, starting with an assumed change in effective dielectric constant alone. Without information to guide the magnitude of expected change in the dielectric constant, it was varied over a large range to gauge the impact on magnitude and phase of $s_{11}/s_{22}$ ($s_{21}$ and $s_{12}$ are unaffected). The simulations show that the phase is indeed affected, particularly at the highest frequencies, as is the magnitude, as is shown in Figure 10- Figure 14. Though there is an effect on phase especially it is a fairly subtle one, considering that actual changes in effective dielectric constant would be much smaller and detecting the change in phase would require fairly precise tuning.

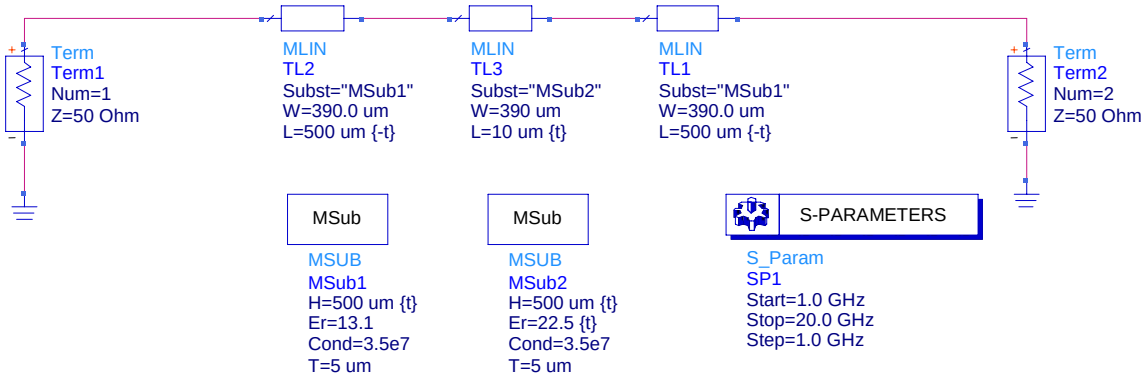


**Figure 9.** Transmission line model for simulation.

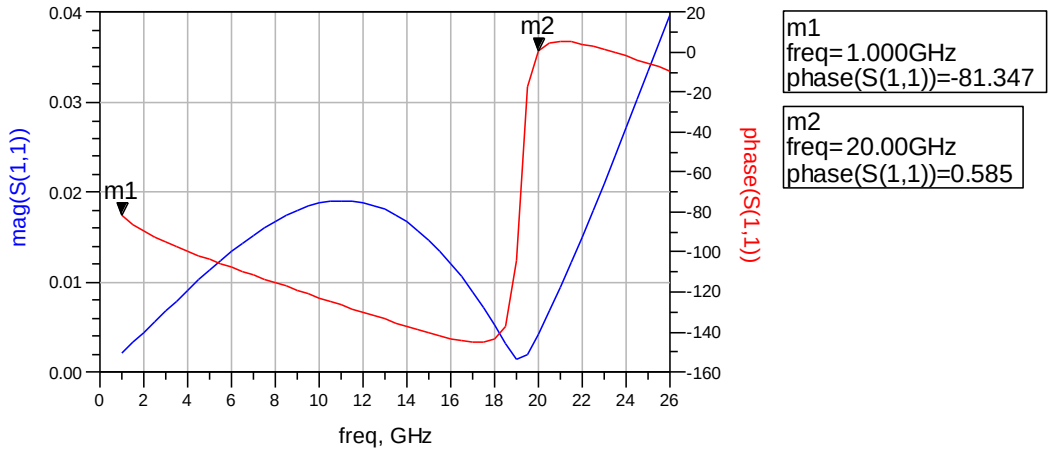


**Figure 10.** s11 for εr=5 for TL3.

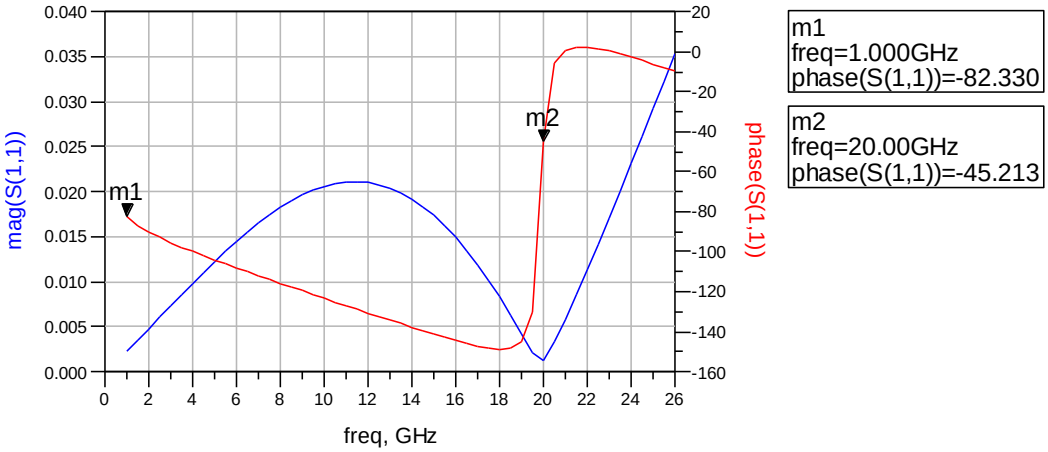


**Figure 11.** s11 for εr=13.1 for TL3.

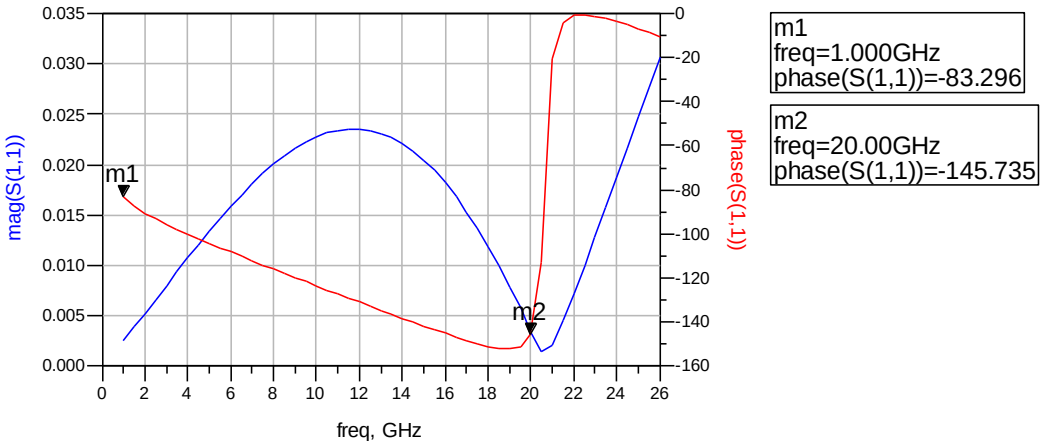


**Figure 12.** s11 for εr=22.5 for TL3.

A perhaps more realistic approach to the simulation is to vary the loss tangent of the dielectric. This is somewhat more reasonable since while it is hard to know how the dielectric constant would be affected, it is well-known that the presence of charge carriers will definitely make a substrate more lossy. In fact, the relative lack of carriers in undoped GaAs is a large part of what makes it a superior substrate for microstrips than materials such as Si, which is more conductive. Once again, there is little to guide us on how much the loss tangent can be expected to change without three-dimensional electromagnetic simulation, so we have used a range of 0 (ideal) to 0.45, which is a quite high loss tangent for an ordinary high-frequency substrate, but smaller than what would be encountered for ordinary (10 Ω-cm) Si at high frequency [17]. The results for this are somewhat different, as shown in Figure 15-Figure 15, below.

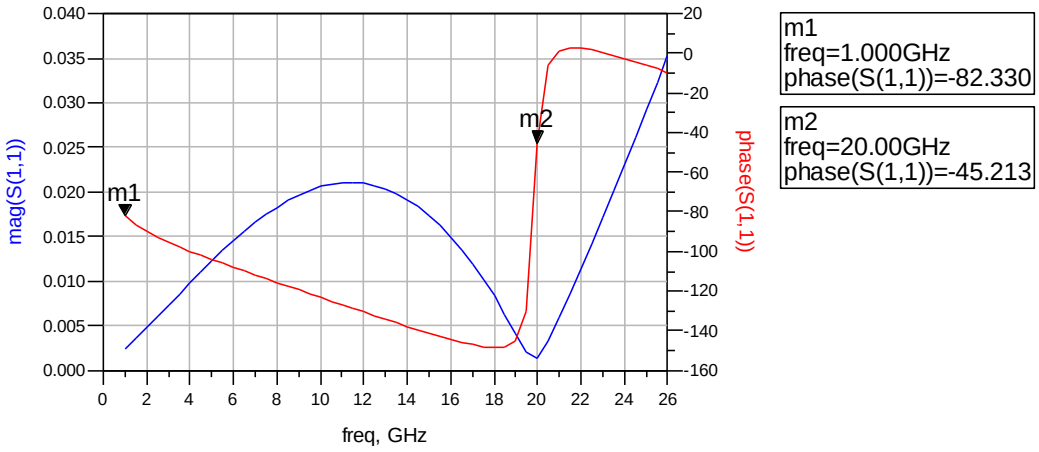


**Figure 13.** s11 for loss tangent=0 for TL3.

.

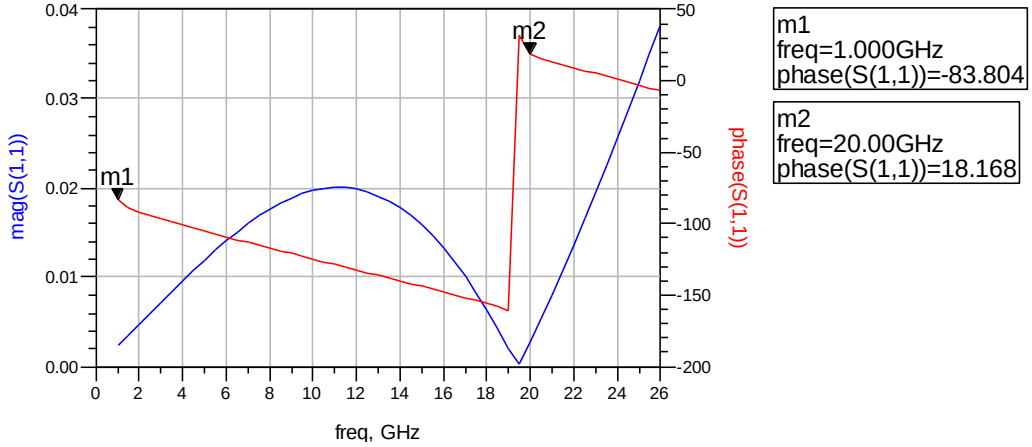


**Figure 14.** s11 for loss tangent=0.2 for TL3.

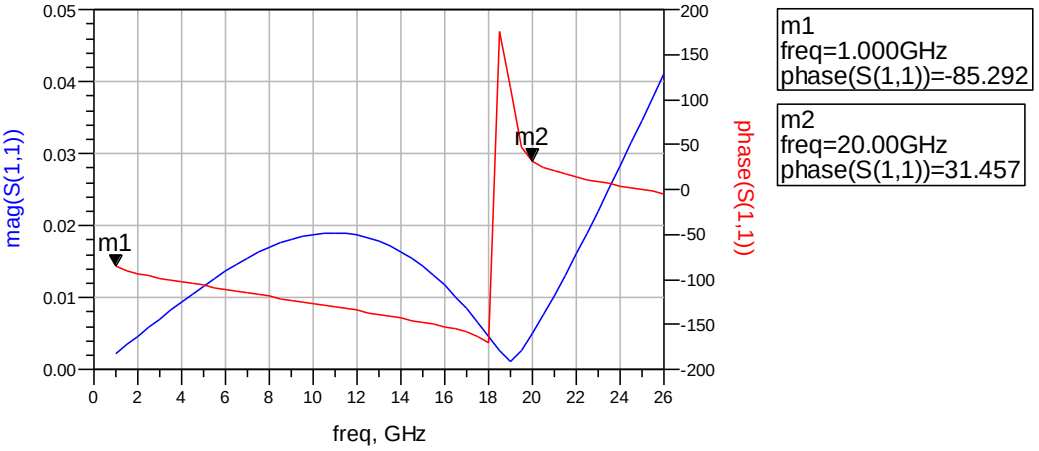


**Figure 15.** s11 for loss tangent=0.4 for TL3.

Both simulation approaches reveal that, even under what are probably optimistic assumptions, the effects are fairly subtle unless precisely tuned, which may not be realistic. The most optimistic element in this simulation is probably the necessary (due to the limitations of this type of simulation) one that the entire width of transmission line is equally affected, when in reality is probably only a small portion of it that is. The primary missing piece is how to tie this to physically realistic parameters. The assumptions guiding modeling of the actual physical effects were crude and rather arbitrary, so it is hard to know if they are very close to reality. Therefore, the next steps would involve collecting empirical information, physical simulation or both to better bound the problem. In particular, we need to know the approximate volume of material that would be affected, the time scale of the effect and how it manifests in terms of dielectric loss. Getting even an order of magnitude approximation of these things would allow more detailed physical simulation to better understand if the geometry of a transmission line can be designed to actually be sensitive to the effects.

## Capacitor Transients

A second approach is related to that of the transmission line, but deals with the circuit as discrete lumped elements. The notion here is that a detector cell is made out of parallel conducting plates and a suitable, radiation-sensitive dielectric such as liquid Xe, which together comprise a simple capacitor. Rather than taking the traditional approach of biasing the plates to separate radiation-generated charge and collecting it at as a transient current on the plates, this approach attempts to use transient changes in the capacitor behavior for detection.

To simulate such a scenario, two approaches were used. The first approach uses transient simulation with a current pulse to simulate the track of charge generated within the capacitor while it is in a simple circuit with a high-frequency sinusoidal signal applied. The capacitor's resistive loss is modeled as a shunt resistor. Choosing a representative capacitance is somewhat arbitrary but with the following guidelines in mind. The relative permittivity of liquid Xe is quite low (about 1.96 [18]), so even large geometries result in fairly low capacitance. Even values as low as 1 pF require a plate area of 288 $mm^2$ with a plate separation of 500 µm. This, in turn, means that low valued capacitive cells may be constructed with dimensions that are large by photolithography standards. The majority of simulations used a capacitance of 100 fF, which corresponds to 17 $mm^2$ plates.

The complete circuit used in these simulations is shown in Figure 16 below. In this circuit the inductors represent bond wires, the current source was used for transient current pulses and the small circuit at the top was used for a reference signal to compare to the simulated circuit's signal to better see deviations from the transient effects. For s-parameter simulations, which require a steady-state solution, the transient source is ignored, so the state of s-parameters must be examined for different values of shunt resistance, much as was done with transmission lines.

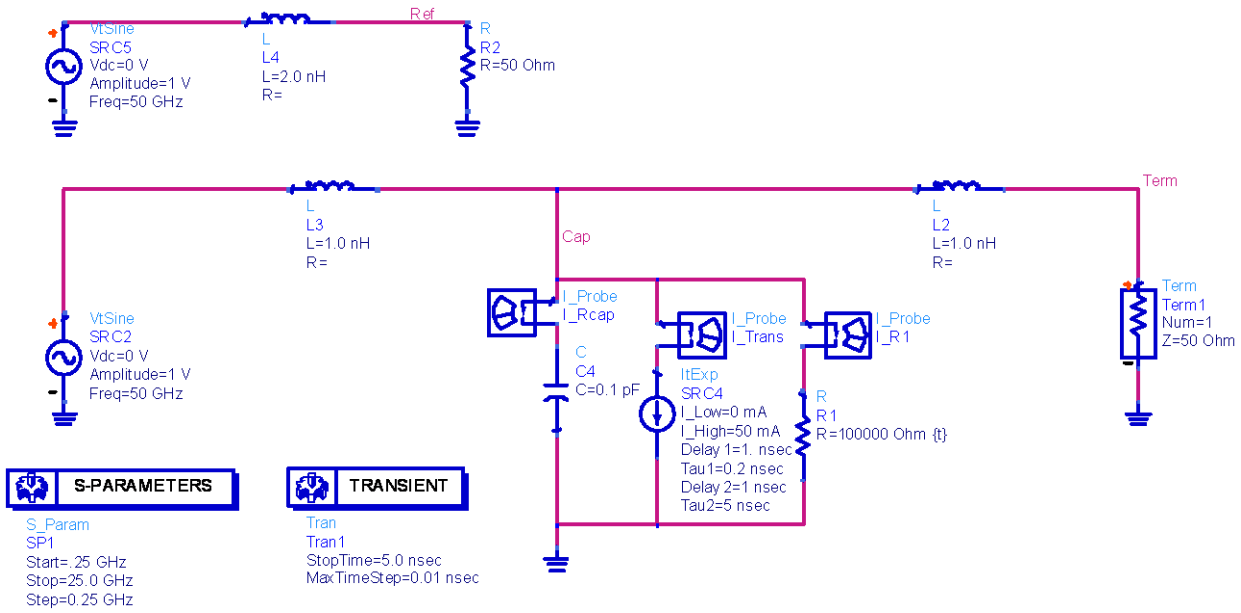


**Figure 16.** Circuit used for capacitor simulations.

For the transient current source, a rise time constant of 200 ps was used with a decay time constant based on a minority carrier lifetime of 5 ns, though we have no data on minority carrier lifetime in liquid Xe (these simulations showed that as long as either the rise or fall time is fast, long time constants are not important). In the transient simulations, it was clear than the current pulse would cause a short-term change in the transmission characteristics of the capacitor. To see this more clearly, plots were created by either mixing the reference signal with the output signal of the circuit or by subtracting the output signal from the reference signal, both of which could be accomplished by circuits means to produce a distinct signal.

After varying frequency, pulse magnitude and capacitance, several things became apparent. First was that the current rise causes a drop in capacitor voltage and a shift in phase until the pulse peaks. At low frequencies these effects would depend on the phase of signal at the start of the pulse, but for higher frequencies (where rise time is at least five times longer than the period of the signal, and frequencies near resonance are avoided), the effect is much more repeatable, leading to the second observation: signal period needs to be short compared to pulse rise time. For the rise time constant of 200 ps, this meant a signal frequency of more than 30 GHz. This is shown in Figure 17- Figure 19.

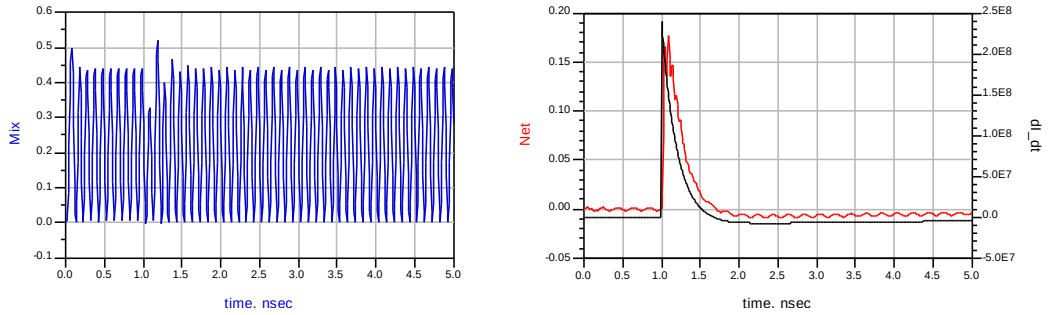


**Figure 17.** Mixed and subtracted signal at f = 5 GHz, with derivative of current transient for reference.

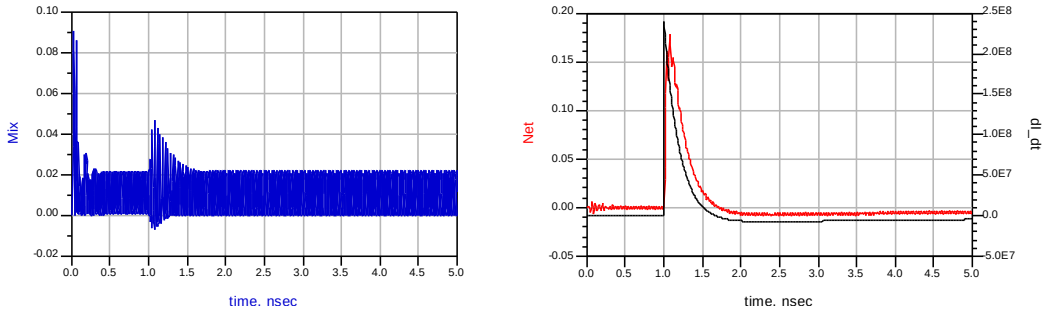


**Figure 18.** Mixed and subtracted signal at f = 30 GHz, with derivative of current transient for reference.

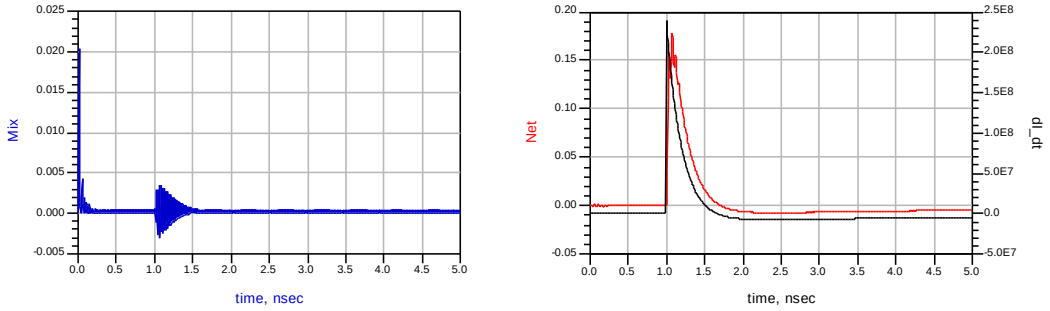


**Figure 19.** Mixed and subtracted signal at f = 50 GHz, with derivative of current transient for reference.

The final observation was that both the mixed and subtracted signals followed an envelope defined by the derivative of current with time. That is, they followed the same magnitude and duration as slope of the current pulse, as shown in Figure 18. This strongly suggests that the parasitic inductors play a key role in creating this transient signal by creating a resonant tank together with the capacitor. This was confirmed by removing inductance from the simulation and observing that there is no signal at all without this. This further suggests that it is important to balance the capacitance with parasitic inductance or added lumped inductance.

Since s-parameter simulation required steady-state circuit behavior, the capacitor's response to radiation had to be approximated by changing its shunt resistor, which represents conductive RF loss in the capacitor. The capacitor resistance scales inversely with the capacitance, meaning that the value at which the shunt resistance becomes important is higher for smaller capacitances, but also has a higher intrinsic value. At high values of $R_{shunt}$ (R1 in the circuit diagram), the s-parameters are insensitive to changes, as expected. The strength of resonance seen in $s_{11}$ magnitude is the primary change, not the resonant frequency or the phase. At some lower value, where $R_{shunt}$ begins to have a non-negligible contribution to the total impedance, the phase of $s_{11}$ starts to be strongly affected at high frequencies. This transition, in this case, occurs at $R_{shunt}$ of about 500 Ω, which corresponds to the equivalent transient current peak of 2 mA, at which the phase signal in the transient simulation begins to have a noticeable effect. For lower $R_{shunt}$ values, the high frequency phase suddenly changes by nearly 360°, while the low frequency phase changes little, except at very low values, as shown in Figure 20-Figure 23.

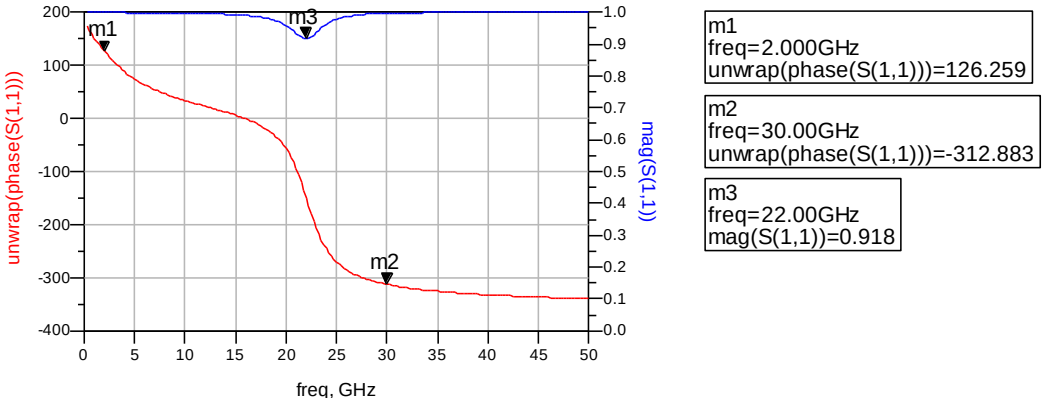


**Figure 20.** s11 for Rshunt = 10000 Ω. Marker m1 shows low frequency phase, m2 shows phase at 30 GHz (above the resonance frequency) and m3 shows magnitude at the intrinsic resonant frequency of about 22 GHz.

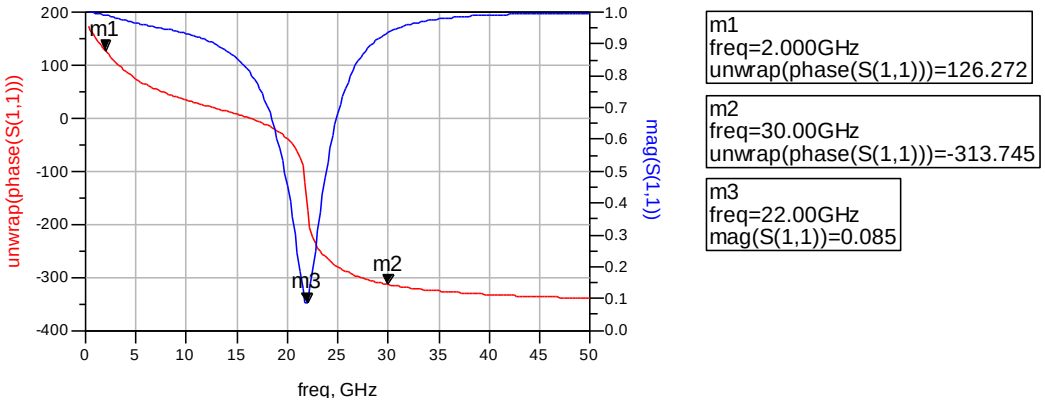


**Figure 21.** s11 for Rshunt = 500 Ω. Marker m1 shows low frequency phase, m2 shows phase at 30 GHz (above the resonance frequency) and m3 shows magnitude at the intrinsic resonant frequency of about 22 GHz.

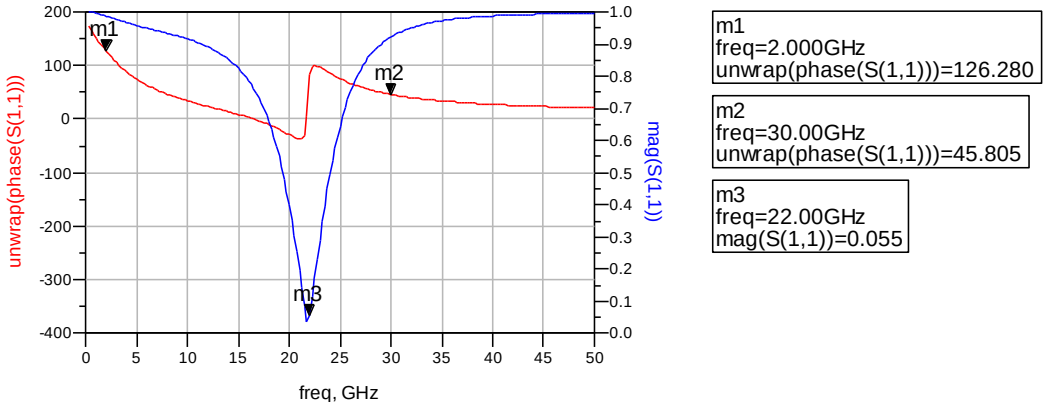


**Figure 22.** s11 for Rshunt = 400 Ω. Marker m1 shows low frequency phase, m2 shows phase at 30 GHz (above the resonance frequency) and m3 shows magnitude at the intrinsic resonant frequency of about 22 GHz. Note that resonant frequency is beginning to shift.

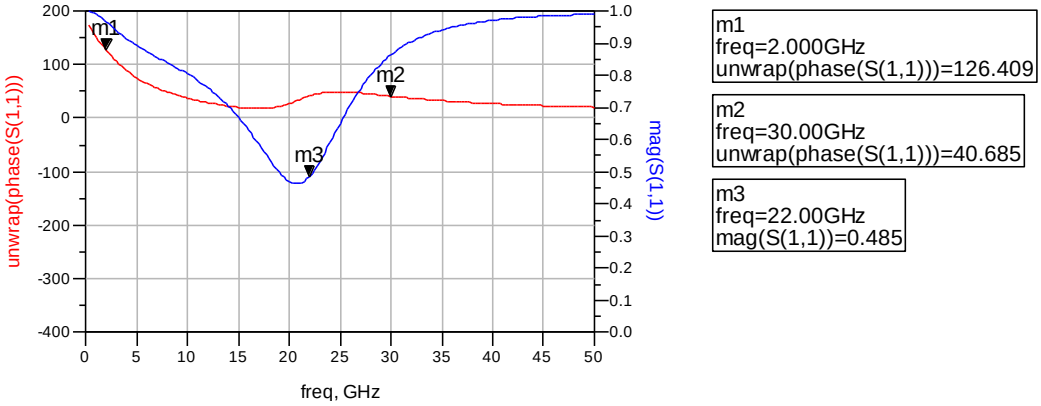


**Figure 23.** s11 for Rshunt = 150 Ω. Marker m1 shows low frequency phase, m2 shows phase at 30 GHz (above the resonance frequency) and m3 shows magnitude at the intrinsic resonant frequency of about 22 GHz.

These simulations, therefore, indicate that a high-frequency phase detector could be used to detect the transient effects of radiation, if the induced charge is enough to sufficiently affect the loss in the capacitive cell. The magnitude of the expected effect is the chief unknown, and would have a large impact on the sizing of capacitive cells. Therefore, quantifying the expected effects of different forms of radiation is the main area that needs to be explored to better determine the practicality of this approach, but is outside the scope of this work.

In summary, both methods show a possible way to detect radiation-induced charge without having to directly collect it. In the case of the of transmission lines, the effect is somewhat subtle, but possibly distinct enough with optimized geometry and substrate, provided the unknown magnitudes of the radiation effects are favorable. Using capacitor transients, a discretized version of the transmission line approach, is more promising, in terms of distinctiveness of the generated signal. The ultimate feasibility of the approach again depends on the actual magnitude of the

physical effects of radiation, particularly the details of the rise and fall times, which may already be known by others but were not available for this work.

# 5. CONCLUSIONS

We have conducted a preliminary study of three concepts for radiation detection. For this initial assessment, we have avoided many specifics of the radiation-matter interaction in order to get a first view of what may be feasible. Instead, it was assumed that in some unspecified material, some appreciable amount of charge or molecular excitation was generated locally. Given that excitation, we simply sought to determine if the proposed concept was feasible.

Our investigation into resonant photonic integrated circuits for radiation detection brought forth some interesting possibilities. First off, a very large response is possible within a carrier excitation range that is within the realm of possibility ($10^5$ carriers/um$^3$). On the other hand, the active area for each ring is small, and the ring thickness (no more than a few microns) is small compared to the interaction length of most ionizing radiation of interest. There is the possibility to pack many rings close together and use multiplexing to read out the excitations of each one. The response is not very linear with excitation energy, and the dynamic range may only be about a factor of 10. Due to the use of these rings in high speed optical integrated circuits, they are very well adapted to very fast readout. They may find a particular niche in readout of high radiation fluxes; it is evident that a substantial amount of design to tailor the response to the details of the application is possible.

Our look at resonant microwave absorption methods started out with the realization that standard EPR was not nearly sensitive enough to be used for radiation detection. Using optical detection, this sensitivity can be improved to the needed level – and in fact has been demonstrated down to single spin measurement. However, optical readout methods are ultimately limited to the performance level of scintillators if the optical signal arises from the microwave-induced change in recombination probability of the excited state. Therefore, it would make more sense to improve scintillator materials instead of developing a new technique, unless there were a very clear means to extract either direction information or particle discrimination using ODMR and a particular sensing material. We did not find obvious opportunities in this direction. This brings us back to the resonant photonic circuit; in the resonant ring, the circulating "probe" light has many chances to interact with the excited volume, which leads to the improved sensitivity. Likewise, if trying to sense excited molecules, the sensitivity can only be improved from the scintillator case if the excited state is not destroyed by the probe. Recent literature suggested that excited states can be studied with very high sensitivity using coherent anti-Stokes Raman scattering. While this third-order optical experiment is somewhat complex, continuing improvements in laser sources may soon make this a feasible option for radiation detection. There would be a significant amount of work needed to find the optimum detector material – it would need to have a radical generated by radiation with a large Raman cross section and a lifetime long enough to make it easy to detect but not so long as to degrade the time response. Given the probability that a known scintillator material may work in this application, a CARS survey of those materials would be a valuable next step as a feasibility study.

The small pixel, capacitive change model offers promise for direct measurement of displacement current. Modeling of the circuit and readout system still needs to be completed.

Finally, our look at RF stripline circuits revealed some possibilities. Standard stripline structures are simply too insensitive to provide a reasonable means for detection using any reasonable substrate.

# 6. REFERENCES


1. S. Adachi, Physical Properties of III-V semiconductor compounds. New York: John Wiley & Sons, 1992.
2. K. Oda, et al., "A Wideband Guided-Wave Periodic Multi Demultiplexer With A Ring Resonator For Optical FDM Transmission-Systems," Journal of Lightwave Technology, vol. 6, pp. 1016-1023, Jun 1988.
3. G. Junpeng, et al., "High-Q microring resonator for biochemical sensors," Proceedings of the SPIE - The International Society for Optical Engineering, vol. 5728, pp. 83-92, 2005.
4. E. H. Haskell, et al., "A High Sensitivity EPR Technique For Alanine Dosimetry," Radiation Protection Dosimetry Vol. 77, No. 1/2, pp. 43–49 (1998).
5. A. Anisiriov, et al., "Optical Detection of the ESR Spectrum of Hexafluorobenzene Anion Radicals in Squalane at Room Temperature," Chemical Physics Letters, vol. 73 (1).
6. D. Suter and J. Gutschank, "Laser-Assisted Magnetic Resonance: Principles and Applications," Lecture Notes in Physics, vol. 684. p.115-141 (2006).
7. Stephen A. Payne and R. M. Hochstrasser, "Picosecond transient coherent anti-Stokes Raman spectroscopy of Rhodamine 560 in ethanol," Optics Letters, Vol. 11, Issue 5, pp. 285-287 (1986).
8. X. Xie et al., "Living Cells as Test Tubes," Science, vol. 312 no. 5771, pp. 228-230, 2006.
9. H. Ichinose, T. Doke, J. Kikuchi, A. Hitachi, K. Masuda and E. Shibamura, Nucl Instrum Meth A 305 (1), 111-115 (1991).
10. T. Takahashi, S. Konno, T. Hamada, M. Miyajima, S.Kubota, A. Nakamoto, A. Hitachi, E. Shibamura and T. Doke, Phys . Rev. A12 (1975) 249.
11. ICRU Report (1984) 37 : The range of an electron isderived from the same way as that of an a-particle .
12. J.F. Ziegler, He, Stopping Powers and Ranges (Pergamon,Oxford, 1977): the range of an a-particle in liquid rare gas is derived from the density of 3.0 g/cm3 for liquid Xe and 1.4 g/cm3 for liquid Ar.
13. ASTAR. http://physics.nist.gov/cgi-bin/Star/ap_table.pl
14. http://electronicdesign.com/article/analog-and-mixed-signal/measure-capacitive-sensors-with-a-sigma-delta-modu.aspx
15. RF Cafe - Microstrip Substrate Equations Formulas, http://www.rfcafe.com/references/electrical/microstrip-eq.htm, modified July 18, 2010.
16. S.M. Sze, *Physics of Semiconductor Devices*, New York: John Wiley & Sons, 1981.
17. R.-Y. Yang, et. al, "Loss Characteristics of Silicon Substrate with Different Resistivities," *Microwave and Opt. Tech. Lett.*, vol. 48 (9), pp. 1773-1776, Sept. 2006.
18. Enrico Conti's Liquid Xenon Page, http://www.pd.infn.it/~conti/LXe.html, modified June 22, 2010.

# DISTRIBUTION

| | | | |
|---|---|---|---|
| 1 | MS1080 | Mark Derzon | 1749-2 |
| 1 | MS1085 | Michael Cich | 1742 |
| 1 | MS1085 | John Martinez | 1742 |
| 1 | MS1085 | Chris Nordquist | 1742 |
| 1 | MS1085 | Olga Spahn | 1742 |
| 1 | MS1085 | Allen Vawter | 1742 |
| 1 | MS9406 | Lorraine Sadler | 8132 |
| | | | |
| 1 | MS0899 | Technical Library | 9536 (electronic copy) |
| 1 | MS0123 | D. Chavez, LDRD Office | 1011 |


Sandia National Laboratories